

Electron-phonon relaxation time in ultrathin tungsten silicon film

M. Sidorova*

*Physics Department, Moscow State Pedagogical University, Russia
and DLR Institute of Optical Systems, Rutherfordstrasse 2, 12489 Berlin, Germany*

A. Semenov and A. Korneev

*Physics Department, Moscow State Pedagogical University, Russia
and Moscow Institute of Physics and Technology, Russia*

G. Chulkova

*Physics Department, Moscow State Pedagogical University, Russia
and National Research University Higher School of Economics, Russia*

Yu. Korneeva

Physics Department, Moscow State Pedagogical University, Russia

M. Mikhailov

*B. Verkin Institute for Low Temperature Physics and Engineering of the National Academy of Sciences of
Ukraine, Kharkiv, Ukraine*

Yu. Devizenko

National Technical University "Kharkiv Polytechnic Institute", Ukraine

A. Kozorezov

Department of Physics, Lancaster University, United Kingdom

G. Goltsman

*Physics Department, Moscow State Pedagogical University, Russia
and National Research University Higher School of Economics, Russia*

*Mariia.Sidorova@dlr.de

Using amplitude-modulated absorption of sub-THz radiation (AMAR) method, we studied electron-phonon relaxation in thin disordered films of tungsten silicide. We found a response time $\tau_R \sim 800$ ps at critical temperature $T_c = 3.4$ K, which scales as T^{-3} in the temperature range from 1.8 to 3.4 K. We discuss mechanisms, which can result in a strong phonon bottle-neck effect in a few nanometers thick film and yield a substantial difference between the measured time, characterizing response at modulation frequency, and the inelastic electron-phonon relaxation time τ_{e-ph} . We estimate the electron-phonon relaxation time to be in the range $\tau_{e-ph} \sim 100-200$ ps at 3.4 K.

I. INTRODUCTION

Since the demonstration of the first Superconducting Single-Photon Detector (SSPD) [1] more than a decade ago many research groups around the world have attempted to improve SSPD performance. Different chip designs and superconducting materials were studied. At present, SSPDs play an important role in the broad areas of applications where single-photon detection is of prime importance [2]. SSPDs demonstrate ultrafast timing performance, i.e. picosecond timing jitter [3] and nanosecond reset time, record detection efficiency [4], ultralow noises and wide spectral sensitivity from visible to near

infrared wavelengths [5]. The most recent advance was achieved with SSPD based on amorphous superconductor tungsten silicide (WSi) that allowed the development of a device with a record detection efficiency exceeding 90% [6]. Nevertheless, at present real devices fail to combine record performance metrics at the same time. The main reason why this has not been achieved yet is the absence of complete understanding of the detection mechanism.

The detection mechanism in SSPD is connected with the formation of resistive state in current-carrying superconducting nanowire. It is triggered by the absorption of a photon. Whilst the exact origin of the resistive state is important and was the subject of extensive recent theoretical works [6-9], the no less important problem of the initial excited state in the current-carrying superconducting nanowire was not studied in detail. The excited state is created in the energy down-conversion process following photon absorption and initial energy deposition in the form of energetic electronic excitations. From initial electronic excitations it proceeds via an avalanche-type cascading process characterized by a multiplication of the number of carriers and phonons with continuous spectral downslide, until the excited volume containing highly non-equilibrium quasiparticles and phonons, termed as a hotspot, is formed. Recently, it was shown that the evolution of hotspot in current carrying nanowire while it remains superconducting can be studied in detail in a two-photon detection regime [10-11]. In experiments with two-photon detection Marsili et al. [10] tuned the operation conditions of SSPD (bias current, energy of photons and bath temperature) in such a way that the energy of a single photon was not sufficient to create a hotspot capable of destroying superconductivity, but the absorption of two photons results in a detection click, provided that the absorption sites are close and the resulting hotspots overlap, and that the second photon arrives before the first hotspot relaxes. Varying the delay time between the two photons, Marsili et al. measured the dependence of the detection probability as a function of this time for different bias currents over a two photon detection range, photon wavelengths and bath temperature. The detection probability decreased with the delay time, reflecting relaxation of the first hotspot. Thus, the hotspot produced by the second photon was used as a probe to measure the state of relaxation of the first one. Characteristic relaxation time of order of hundreds of picoseconds was found. Kozorezov et al. [11] developed a theoretical model of the hotspot relaxation process based on data from Ref. [10] and showed that most of the relaxation is accounted for by the self-recombination of non-equilibrium quasiparticles within the hotspot with small extra contributions from their diffusion and the cooling of the hotspot due to expansion. The authors [11] used the two-phonon model for simulation of experiments, and assuming that the hotspot is a uniform area of suppressed order parameter with a size determined by the width of the strip, they were able to describe all the data with only 3 fitting parameters, the energy deposition efficiency, δ , describing the excitation level in the hotspot and depending on the fraction of photon energy deposited into electronic system, phonon bottle-necking parameter, γ , and characteristic electron-phonon relaxation time τ_0 , which depends on material, and was found to be 0.84 -1.0 ns [10] for WSi. The observed hotspot relaxation times varied over an order of magnitude from few hundred ps to few ns depending on

experimental conditions. Thus, electron-phonon relaxation in WSi turned down to be slow in comparison with conventional SSPD materials, such as NbN and NbTiN (where measured time of relaxation of electron temperature at critical temperature was of the order of 10 ps) [12]. The slower electron-phonon relaxation in WSi in the temperature range close to material critical temperature is of no surprise, being a consequence of lower T_c in WSi in comparison with NbN. The exact strength of electron-phonon interaction in WSi is an important characteristic, not only determining its superconducting properties, but arguably being significant for superior detection capabilities of this material. So far, the strength of electron-phonon interaction was probed in two-photon experiments in extremely non-equilibrium conditions in a superconducting state. Moreover, the theoretical model [11] as many other kinetic models applied to extremely disordered thin WSi film may be greatly oversimplified. As a result, obtaining quantitative information from fitting experimental data to a specific experiment is not easy. Therefore, independent techniques to study the electron-phonon inelastic time in WSi and other prospective SSPD materials providing different data sets are urgently needed.

There are many techniques to study electron-phonon interactions that differ from each other by perturbations induced in the systems of interacting electrons and phonons. They all have their own advantages and disadvantages. The method of determination of electron-phonon relaxation time, τ_{e-ph} in Ref. [10, 11] uses strong model assumptions about the initial geometry of a hotspot and the inefficiency of diffusion. Here we use a method, which allows measurements of τ_{e-ph} in various ultrathin films based on amplitude-modulated absorption of sub-THz radiation (AMAR) introduced by Gershenson et al. [13-15]. Its physical background and conditions of applicability were discussed in a recent paper by Kardakova et al. [16]. In this paper we report measurements of electron-phonon relaxation time in an ultrathin WSi microstrip using this technique. In contrast with the two-photon pump-and-probe technique used by Marsili et al. [10], this technique probes electron-phonon interaction in a normal state slightly above critical temperature. It is essential that the electrons are at a quasi-equilibrium at a temperature, which is marginally higher than the phonon and substrate temperature. Besides, perturbation of the system remains spatially homogeneous, thus excluding effects, which are connected to thermal diffusivity. Determination of energy relaxation time due to electron-phonon interaction from data depends on the accurate assessment of the phonon bottle-neck effect. Although the same effect is equally important in a two-photon detection experiment, the values of τ_0 derived from the dataset [10] were shown to be less sensitive to the phonon bottle-necking parameter [11].

II. THIN FILM TECHNOLOGY AND EXPERIMENTAL METHOD

The experiments in this work were performed on a microstrip fabricated from a superconducting WSi film. The WSi film (atomic ratio W:Si=3:1 calibrated by sputtering rate of individual components) was deposited by dc magnetron sputtering in argon onto thermally oxidized silicon wafers. The substrate was placed onto a rotatable holder and the holder was alternately

positioned over pure tungsten and pure silicon targets for sequential deposition of ultrathin W and Si layers with such a rate that the deposition of WSi film of thickness $d = 3.4$ nm was completed after seven revolutions. The film was capped with a 4 nm thick Si layer to prevent oxidation. During sputtering the substrate was kept at room temperature. Transmission electron microscopy analysis of the deposited film showed that the film is amorphous. The film was patterned into a microstrip of the width $w = 1$ μm and length $L = 10$ μm using electron-beam lithography and placed between V-Cu contact pads. The critical temperature of the patterned film was 3.4 K, and the width of resistive transition was 0.25 K.

We studied electron-phonon energy relaxation using the AMAR method [14-16]. The superconducting microstrip was kept at the superconducting transition, biased with small DC current, and exposed to amplitude-modulated radiation of submillimeter range. The absorption of incident radiation power caused an increase of electron temperature and consequently resulted in an increase of the sample resistance producing the change of the voltage signal. The amplitude of the voltage signal exhibited frequency-dependent roll-off (inset of spectrum analyzer on Fig.1), which was used as an indicative of sample response time, which is connected with the intrinsic energy relaxation time. The measured response time coincides with the electron-phonon relaxation time if phonons of the film act as a thermal bath. If this condition is not satisfied, then the response time is affected by phonon reabsorption. The electron-phonon relaxation time can still be extracted. However, an accurate analysis is more complicated, and other parameters entering the model must be assessed independently.

The experimental setup is shown in Figure 1. The sample was mounted on a waveguide flange and placed in a liquid helium cryogenic insert that allows operation at a temperature range down to 1.8 K. The temperature was registered by a carbon thermometer in close vicinity to the sample. The measurements were performed using the oscillation beats of two backward wave oscillators (BWOs), as a source, operating at close frequencies in the range of 120-145 GHz [14]. The radiation of both the local oscillator (LO) and signal BWOs was coupled by 50/50 beam splitter passed through a waveguide (with an included polarization controller) to the sample. If the two signals from BWOs have close frequencies f_{1BWO} and f_{2BWO} , the stream of RF power irradiating the sample has oscillations at intermediate frequency (IF), $f_{IF} = |f_{1BWO} - f_{2BWO}|$. The tuning of IF was realized by changing the frequency of LO, while the frequency of signal oscillator remained constant. Using an attenuator we adjusted the radiation power of the LO BWO. Since the LO power depends on frequency, we re-tuned LO power every time the frequency was changed. The sample response at IF in the range of 5 - 1200 MHz was passed through bias-tee with a separated RF path and the DC voltage bias, amplified, and, together with IF, measured with a spectrum analyzer. The readout path was calibrated directly while measuring.

In experiments, the heating of the electron system by DC and RF power was extremely low and it remained in the quasi-equilibrium regime. It was verified by energy relaxation time being not sensitive to any change in DC and RF power (Fig. 2

(a). The operating point of the sample in the middle of superconducting transition was tuned by a combination of an applied DC voltage bias and radiation power. Maintaining the sample in the middle of superconducting transition by irradiating it by low-power RF radiation and applying small DC current, we measured the response time as a function of DC voltage (Fig. 2 (a) red fill points). Having found the range of voltages where this time doesn't depend on voltage, we then chose the voltage value within this range, at which the output signal is maximal. At this voltage value fixed we then measured the response time by varying RF radiation power (Fig.2 (a) blue empty points). As a result, we found the range of RF powers, where the response time does not depend on RF power. Finally we chose the RF power level within this range, where the output signal has the highest value. At such a regime we carried out all measurements of energy relaxation. Current-voltage characteristics of the microstrip are plotted in Figure 2 (b), where the solid blue curve is obtained in a superconducting state at a low temperature (1.8 K) and the dashed black curve (the operating IV curve) is obtained at the temperature of the superconducting transition with applied RF power.

The typical spectrum of the sample response at IF is shown in the inset to spectrum analyzer of Figure 1. The spectrum has the expected plateau for low frequencies and a roll-off towards higher frequencies. To extract the relaxation time, we fitted the frequency dependence of the response according to the expression

$$\delta U(f) = \delta U(0) \left(1 + \frac{f^2}{f_{3dB}^2}\right)^{-1/2}, \quad (1)$$

with fitting parameters $\delta U(0)$ and $f_{3dB} = 1/(2\pi\tau_R)$ corresponding to 3dB roll-off frequency of the response.

To study the temperature dependence of τ_R we shifted the transition temperature T_c by applying a magnetic field perpendicular to the sample surface. As demonstrated in Fig. 3a, the applied magnetic field shifts the spectral curves (which are fitted using the Eq. (1)) to lower frequencies, hence resulting in increasing τ_R . To create the magnetic field we used a superconducting solenoid mounted together with a cryogenic insert into He-Dewar (Fig.1). The measured temperature-dependent relaxation time is shown in Figure 3.b. This dependence can be fitted by the power law as $\tau_R \sim T^{-n}$. We found $n = 2.87 \pm 0.18$, which can be identified with the integer value $n=3$.

To compare the obtained results with the theoretical prediction we also carried out measurements of the electron diffusion constant, D , and electron density of states at Fermi level, $\nu(0)$, which are used in the calculations of the hotspot dynamics [6]. D is obtained from the dependence of the second critical magnetic field, H_{c2} , on temperature close to T_c . The introduction of the magnetic field leads to a reduction of the critical temperature and a widening of the transition, shifting the

$R(T)$ curves to low temperatures (inset of Fig.4). The sample was biased with a small alternating current, which didn't cause any noticeable heating of the electron subsystem. For each value of H_{c2} , we defined the temperature of the superconducting transition using a point at which the resistance of the films becomes half of the normal state value. The applied magnetic field was interpreted as a second critical field, H_{c2} , at this temperature (Fig. 4). The diffusion constant was calculated according to the practical formula [17]:

$$D = 1.097 \left(-\frac{dH_{c2}}{dT} \right)^{-1} \Big|_{T=T_c}. \quad (2)$$

The derivative of the second critical magnetic field dH_{c2}/dT was calculated as a slope of a line fitting the linear part of the dependence, see Fig.4. The calculated value D for the WSi thin film is $0.58 \text{ cm}^2/\text{s}$.

The electron density of states at the Fermi level was estimated using experimentally determined values of the electron diffusion constant and the resistivity according to Einstein relation $\nu(0)=1/(e^2\rho D)$, and found to be $5.3 \times 10^{22} \text{ eV}^{-1} \text{ cm}^{-3}$.

In Table 1 we summarize all measured parameters, for WSi. R_{\square}^{300K} is the sheet resistance at room temperature (300K), the resistivity was determined from the sheet resistance and film thickness, d , as $\rho^{300K}=d R_{\square}^{300K}$. The critical current density was calculated using data of the critical current of $35.2 \text{ }\mu\text{A}$ at temperature 1.8K (solid blue curve Fig.4).

TABLE I. Parameters of the WSi film sample.

d , (nm)	L , (μm)	w , (μm)	T_c , (K)	dT_c , (K)	R_{\square}^{300K} , (Ω / \square)	ρ^{300K} , ($\Omega \text{ cm}$)	$jc (T=1,8K)$, (A / cm^2)	D , (cm^2 / s)	τ_R at T_c , (ns)	$\nu(0)$, ($\text{eV}^{-1} \text{ cm}^{-3}$)
3.4	10	1.0	3.4	0.25	595	2.02×10^{-4}	1.04×10^6	0.58	0.8	5.3×10^{22}

In order to discuss and interpret our data, first we stress that the measured relaxation time is an intrinsic property of the relaxation processes in the film, and is practically unaffected by the electro-thermal feedback (ETF), in contrast to the transition edge sensors (TES) [18]. To estimate the correction due to ETF, we use the formula:

$$\tau_{etf} = \frac{\tau_R}{1+L_0/(1+\alpha_I)}. \quad (3)$$

In our case, the correction is determined mainly by a loop gain $\mathcal{L}_0 = P_0\alpha_T/GT_0$, where dissipated power P_0 is expressed through the bias current I_0 , the resistance of the sample at the operation point R_0 and the load resistance R_L as $P_0=I_0^2(R_0-R_L)\rho$ with $\rho=(R_0-R_L)/(R_0+R_L)$; G is the thermal conductance, $\alpha_T = (T/R_0)(dR/dT)$ and $\alpha_I = (I_0/R_0)(dR/dI)$. The load resistance was

50 Ω . From IV curve (the dashed curve on Fig.2.b), $R_0 \approx 1 \text{ k}\Omega$, while from the R(T) curve (inset to Fig.4) we obtain the rough estimate $\alpha_T \approx 10$. Estimating thermal conductance as $G=C_e/\tau_R$, we obtain the negligibly small loop gain factor, $\mathcal{L}_0 \approx 0.05$. The account for the non-zero logarithmic derivative of resistance versus current, α_I , can only decrease the correction. Thus, we neglect the effect of ETF.

III. DISCUSSION

It is worth starting the analysis of experimental data by drawing the expected values of relaxation times in WSi, based on a model of a superconductor with a strong elastic scattering (dirty superconductor model) [19]. It obviously cannot account for possible effects of renormalized electron-phonon interaction in the presence of strong impurity scattering, which can be significant in WSi, and also for reduced dimensionality of phonons in thin film at a low temperature. Nonetheless, it provides some reference prior to a quantitative comparison with the experimental data. In spite of the effect of disorder such an estimate works reasonably well for the case of NbN. To estimate the expected electron-phonon time, one can rewrite the formula [19] for the characteristic time τ_0 as

$$\tau_0 = \frac{1+\lambda}{2\pi\lambda} \frac{\hbar}{k_B T_c} \left(\frac{T_D}{T_c} \right)^2. \quad (3)$$

Comparing the material parameters of WSi with those of the materials listed in [19], one can expect that λ is between 1 and 2. With the Debye temperature $T_D=400 \text{ K}$ and $T_c=3.4 \text{ K}$, one obtains $\tau_0=10 \text{ ns}$ for $\lambda=1$ and 7.5 ns for $\lambda=2$. The corresponding electron-phonon energy relaxation time is $\tau_{e-ph}(T_c) \approx \tau_0/38$ (one can derive this factor assuming that the electron subsystem is in equilibrium at some temperature $T+\delta T$ slightly greater than the phonon temperature T and calculating the relaxation time for δT , see Ref. [19]). This yields $\tau_{e-ph}=260 \text{ ps}$ for $\lambda=1$ and 200 ps for $\lambda=2$. This is several times shorter than the measured relaxation time at T_c .

One of the possible reasons for the discrepancy is the effect of a phonon bottle-neck. To account for this, one should estimate the characteristic phonon-electron time describing phonon re-absorption. As a measure of this time, one can use the time of energy relaxation of the phonon subsystem due to the interaction with the electron subsystem, τ_{ph-e} . In a quasi-equilibrium case (the so-called two-temperature model [21]: both the electron and phonon subsystems of the film at every moment are in their partial equilibriums and described by some temperatures T_e and T_p), it is related to τ_{e-ph} by the energy balance equation $C_e/\tau_{e-ph}=C_{ph}/\tau_{ph-e}$. Estimating C_e within the free-electron model as $C_e=(\pi^2/3)k_B^2\nu(0)T$ and C_{ph} within the Debye model as $C_{ph}=12/5\pi^4 N_a k_B^2 (T/T_D)^3$, where N_a is the number of ions per unit volume, one obtains $C_{ph}/C_e=0.177$ at

$T=T_c$, which yields $\tau_{ph-e}=0.177\tau_{e-ph}=46$ ps for $\tau_{e-ph}=260$ ps. This value is comparable to an estimated phonon escape time $\tau_{esc} \approx 36$ ps if we use the common expression $\tau_{esc} = 4d\alpha^{-1}u^{-1}$, where α is the acoustic transparency of the film–substrate interface, and u is the mean sound velocity. The latter was taken to be close to the mean sound velocity of transverse acoustical modes because of their dominant densities of states at low phonon frequencies, $u \approx 2080$ m s⁻¹. The acoustical impedances of the SiO₂ substrate were estimated using data from [22] for soda-lime glass, sound velocity in the substrate $u' = 3480$ m s⁻¹, hence we estimate $\alpha = 0.2$. Thus, the effect of phonon reabsorption is expected to extend the measured time τ_R compared to τ_{e-ph} . In the quasi-equilibrium case this is described by $\tau_R = \tau_{e-ph}(1 + \tau_{esc}/\tau_{ph-e}) = \tau_{e-ph} + (C_e/C_{ph})\tau_{esc}$, thus the expected value of τ_{e-ph} is $\tau_R - (C_e/C_{ph})\tau_{esc} = 590$ ps at $T=T_c$. It is worth noting that the phonon re-absorption rate, which is important for a phonon bottle-neck is only part of τ_{ph-e}^{-1} , the other part being the phonon scattering rate off electrons, resulting in stronger bottle-necking in comparison with our estimate. Phonon bottle-necking apparently affects the temperature dependence of τ_R , making it different from $\tau_{e-ph}(T)$. It deviates from T^{-3} law because the correcting term in the denominator is proportional to T^{-2} . Numerically, it turns out that in the range of temperatures of the experiment, the resulting dependence of τ_{e-ph} on T extracted from $\tau_R(T)$ with the account for the correcting term, is indistinguishable from the power-law with $n=3$.

In a real situation, the excess phonons are far from equilibrium because of the absence of an efficient intrinsic equilibration mechanism in the phonon subsystem. An account for this will result in an even more pronounced deviation of τ_{e-ph} from τ_R . Within the rough model, where the distribution of non-equilibrium phonons is assumed to be peaked at some energy $\hbar\omega$, the correction to the formula for a quasi-equilibrium case, which was derived above, is the replacement of τ_{ph-e} to some lower value $\tau(\omega)$, the time of absorption of phonon at energy $\hbar\omega$ by electrons at temperature T . Hence, we conclude that the effect of phonon reabsorption can explain at least a part of the difference between the measured relaxation time and the electron-phonon relaxation time following from the model [11].

The expression for phonon escape time $\tau_{esc} = 4d\alpha^{-1}u^{-1}$ can be derived only under the assumption of phonon distribution in the sample remaining fully isotropic at any instance of time. However, in thin films the validity of this assumption may become questionable. Indeed, in a thin film, phonons may traverse the film over the time, which is significantly less than any other scattering times. For example, a phonon moving with a group velocity of $2.08 \cdot 10^3$ m/s traverses 3.4 nm thick film in 1.6 ps. As a result, the majority of phonons with the incidence angles less than the angle of total internal reflection, $\vartheta \leq \vartheta_c$, will pass across the escape interface into the substrate and the whole of conical volume with $\vartheta \leq \vartheta_c$ in the momentum phase space becomes depleted. Phonons initially propagating with wave-vectors outside this conical volume will bounce back and forth within a flat-parallel film until they undergo a scattering-assisted conversion into the conical volume, thus replenishing phonon numbers and contributing to further phonon escape. This latter, however, occurs at a diminished rate, which is

controlled by the rate of conversion. One of the possible conversion mechanisms is the elastic scattering of phonons, either disorder related, or Rayleigh scattering at the interface or surface roughness with the rate τ_s^{-1} , which may not be efficient both because of long wavelength of dominant phonons and (for the case of scattering at interface and surface roughness) due to more oblique incidences, $\vartheta > \vartheta_c$. Another mechanism is the composite conversion, involving an absorption of a phonon from the volume $\vartheta > \vartheta_c$ by the electronic excitations with the rate τ_{ph-e}^{-1} and subsequent instantaneous re-emission (to keep the detailed balance) of another phonon with the changed momentum. For isotropic scattering the latter will result in a conversion with probability, which is proportional to the fraction of the solid angle with $\vartheta \leq \vartheta_c$. Therefore, the conversion rate is $2 \sin^2\left(\frac{\vartheta_c}{2}\right) (\tau_{ph-e}^{-1} + \tau_s^{-1})$. In order to evaluate the phonon bottle-necking denominator more accurately we write down the kinetic equations for phonon distribution $N(\vartheta)$ neglecting phonon diffusion

$$\frac{\partial N}{\partial t} = -(N - \langle N \rangle) \left(\frac{1}{\tau_{ph-e}} + \frac{1}{\tau_s} \right) - \frac{N - N_0(T_0)}{\tau_{esc,0}} f(\vartheta) + N_i \delta(t) [1 - f(\vartheta)], \quad (4)$$

where $\langle N \rangle \equiv \frac{1}{2} \int_0^\pi d\vartheta \sin \vartheta (\dots)$ is the phonon distribution averaged over all angles, $\langle N \rangle_c \equiv \frac{1}{2} \int_0^{\vartheta_c} d\vartheta \sin \vartheta (\dots)$, $N_0(T_0)$ is the equilibrium Planck distribution at the substrate temperature T_0 , $\tau_{esc,0}$ is the escape time from the volume $\vartheta \leq \vartheta_c \cup \pi - \vartheta_c \leq \vartheta \leq \pi$, $f(\vartheta) = \Theta(\vartheta_c - \vartheta) + \Theta(\pi - \vartheta)\Theta(\vartheta + \vartheta_c - \pi)$ and $\Theta(x)$ is the step-function. Phonons falling into volume $\pi - \vartheta_c \leq \vartheta \leq \pi$ move away from the interface converting into volume $\vartheta \leq \vartheta_c$ after reflection from the interface with the Si cap layer. We have also explicitly shown the initial condition in the form of a distribution function N_i outside the escape cone, and all inside states are empty. We have also taken the ‘‘composite’’ collision integral describing the conversion into escape conical volume $\vartheta \leq \vartheta_c$ via phonon interactions with electrons in the form $-\frac{N - \langle N \rangle}{\tau_{ph-e}}$, rather than solving the more complicated system of kinetic equations for interacting electrons and phonons from two different parts of the momentum space. This is a simplification, which works in conjunction with the detailed balance principle allowing a simple solution. Averaging (4) over angles and separately over $0 \leq \vartheta \leq \vartheta_c$ and solving the resulting system of equations we obtain

$$\langle N \rangle(t) = N_0(T_0) \frac{1}{1 + 2 \cos^2\left(\frac{\vartheta_c}{2}\right) \tau_{esc,0} (\tau_{ph-e}^{-1} + \tau_s^{-1})} + N_i \left[2 \sin^2\left(\frac{\vartheta_c}{2}\right) e^{-t/\tau_{esc,0}} + \left(1 - 2 \sin^2\left(\frac{\vartheta_c}{2}\right)\right) e^{-2 \sin^2\left(\frac{\vartheta_c}{2}\right) (\tau_{ph-e}^{-1} + \tau_s^{-1}) t} \right]. \quad (5)$$

It follows from (5) that the effective phonon escape time is $\tau_{esc} = \frac{1}{2 \sin^2\left(\frac{\vartheta_c}{2}\right) (\tau_{ph-e}^{-1} + \tau_s^{-1})}$ so that for $\tau_{ph-e}^{-1} \gg \tau_s^{-1}$ we

have $\tau_{esc} = \frac{\tau_{ph-e}}{2 \sin^2\left(\frac{\vartheta_c}{2}\right)}$. For this case taking $\vartheta_c = \arcsin\left(\frac{u}{u'}\right) \approx 37^\circ$ we finally estimate

$$\tau_{e-ph} = \tau_R \left(1 + \frac{\tau_{esc}}{\tau_{ph-e}}\right)^{-1} = \tau_R \left(1 + \frac{1}{2\sin^2\left(\frac{\theta_c}{2}\right)}\right)^{-1} \approx \frac{1}{6} \tau_R \quad (6)$$

which gives $\tau_{e-ph}=130$ ps at T_c . The ratio $\frac{\tau_{esc}}{\tau_{ph-e}} = \frac{1}{2\sin^2\left(\frac{\theta_c}{2}\right)}$ does not depend on temperature. Therefore, the T -dependencies of $\tau_{e-ph}(T)$ and $\tau_R(T)$ are identical.

The same conclusion can be arrived at through slightly different reasoning. We introduce two groups of phonons, escaping (1) and non-escaping (2), with temperatures T_{ph1} and T_{ph2} . They are assumed to be isolated from each other and interacting only with the electrons with the effective temperature T_e , and, (for the escaping phonons) with the substrate, which is considered as a heat bath with the temperature T_0 . The heat-balance equations read:

$$\begin{aligned} \frac{dT_e}{dt} &= P_{in} - \frac{T_e - T_{ph1}}{\tau_{e-ph1}} - \frac{T_e - T_{ph2}}{\tau_{e-ph2}} \\ \frac{dT_{ph1}}{dt} &= \frac{T_e - T_{ph1}}{\tau_{ph-e}} - \frac{T_{ph1} - T_0}{\tau_{esc}} \\ \frac{dT_{ph2}}{dt} &= \frac{T_e - T_{ph2}}{\tau_{ph-e}} \end{aligned} \quad (7)$$

Here, $\tau_{e-ph_{1,2}}^{-1} = G_{1,2}/C_e$, and $\tau_{ph-e}^{-1} = G_1/C_{ph1} = G_2/C_{ph2}$, with $G_{1,2}$ the thermal conductances between the electrons and the corresponding phonon groups, and $C_{ph_{1,2}}$ their heat capacities; P_{in} is the incoming power, which heats up the electron subsystem. The specific heats and conductances are proportional to the number of escaping and non-escaping phonons, i.e. $C_{ph1}/C_{ph} = G_1/G = \Omega_1/4\pi$, $C_{ph2}/C_{ph} = G_2/G = \Omega_2/4\pi$, where $\Omega_{1,2}$ are solid angles describing these escaping (1) and non-escaping phonons (2). Comparing the equations for the electrons and for non-escaping phonons, one sees that, in the case $\tau_{ph-e}^{-1} \gg \tau_{e-ph_{1,2}}^{-1}$ (which corresponds to experiment), the condition $T_e - T_{ph2} \ll T_e - T_0$ must be satisfied. Hence, one can omit the third equation and the last term in the first equation, thus returning to modified equations of the two-temperature model for the electrons and escaping phonon. The modification is, that instead of τ_{e-ph}^{-1} the factor $C_{ph1}/C_p = \Omega_1/4\pi = 1/5$ smaller rate must be used. Physically, this means that the electrons and non-escaping phonons form a unified subsystem, which is cooled down only due to the interaction with the subsystem of escaping phonons. Thus, in ultrathin films the phonon bottle-neck effect is enhanced due to the slow replenishing of phonon states within the escape cone.

The above analysis is quantitatively correct in the 3D case, i.e. when the characteristic wavelength of the phonons is small compared to the film thickness. This is not satisfied for the film under consideration, of thickness 3.4 nm: the characteristic wavelength of thermal phonon is $\lambda_T \approx 2\pi\hbar v_s / 3k_B T \approx 15$ nm, if one estimates it as for 3D case. Moreover, the appropriate vibrational modes are not the free standing slab modes, but phonons in the thin film on semi-infinite

substrate. The latter involve truly 3D shear transverse waves, Love- and Rayleigh waves. This indicates that the actual phonon modes structure plays a significant role in electron-phonon interactions and energy relaxation. We also may expect that the bottle-neck effect for Love- and Rayleigh phonons is more pronounced than for bulk phonons, because of the impossibility for a wave propagating parallel to the film-substrate interface to convert into a bulk elastic wave escaping into the substrate because of phase mismatch.

Finally, another reason for the remaining difference between our estimates for τ_0 and the estimate in [11] can be a quantitative inapplicability of the model [11] to ultrathin and disordered WSi films. It is known that in such films, the electron-phonon interaction is significantly modified compared to clean materials, which also results in anomalous temperature dependencies of relaxation time [14, 23, 24]. The coincidence of the power exponent $n=3$ in the temperature dependence of relaxation time in our measurements with the result of a clean limit model (for a bulk sample) can, in principle, be accidental, because of the above-mentioned fact that the phonon subsystem of WSi film of the thickness 3.4 nm at temperature 3.4 K is not fully described by a 3D case. The $n \approx 3$ obtained in the measurements can be due to interplay between disorder-modified electron-phonon interaction and effective lowering of the phonon subsystem dimensionality. At the moment there is no consensus about the applicability of existing theories of disorder-modified electron-phonon interaction [25, 26] to real experimental systems (see, for instance, discussion in Ref. [27]). As a speculation, we note that the value $n=3$ is consistent with the theory [26] and the effective dimensionality 2. In the case when the electron mean free path, ℓ , is small compared to λ_T , which is fulfilled in amorphous WSi film, the theory predicts $n=4$ for a bulk sample, and should yield $n = 3$ for a 2D spectrum of the phonons in the film. The theory [26] (if to neglect phonon bottle-neck effect) also predicts a weakening of the electron-phonon interaction for the case $\ell \ll \lambda_T$ in comparison with the clean case and correspondingly an increase of τ_{e-ph} , which is in line with our observations. The absence of a theory of disorder modified electron-phonon interactions and phonon-bottle-neck in thin films with 2D phonons is the major challenge preventing a more definitive determination of electron-phonon interaction in such a system.

IV. CONCLUSIONS

In summary, we characterized WSi films as a material for developing SSPD. We have shown that in spite of strong disorder in thin WSi film, the effect of a phonon bottle-neck may be substantial. Phonon bottle-necking is likely to occur due to a weak isotropisation of phonon distribution and results in the measured response time of 800 ps significantly slower than intrinsic electron-phonon relaxation time of the order 150 ps.

ACKNOWLEDGMENTS

The work was supported by the Ministry of Education and Science of the Russian Federation, contract No. 14.B25.31.0007, by Russian Foundation for Basic Researches, grant No. 16-29-11779 ofi_m, and also was implemented in the framework of the Basic Research Program at the National Research University Higher School of Economics (HSE) in 2016, project T3-96. M.S. acknowledge the support by Russian Foundation for Basic Researches (grant No. 16-32-00653 mol_a), A.S. acknowledges the support by the State task for institutions of higher education (project No. 2575), G.G. acknowledges the support by the State task for institutions of higher education (project No. XXXX), A.Kozorezov gratefully acknowledges financial support from the Engineering and Physical Sciences Research Council (UK). The authors thank T. M. Klapwijk and D. Yu. Vodolazov for discussion of the results.

References

- [1] G. N. Gol'tsman et al., Appl. Phys. Lett. **79**, 705 (2001).
- [2] C. M. Natarajan, M. G. Tanner and R. H. Hadfield, Supercond. Sci. Technol. **25**, 063001 (2012).
- [3] A. Pearlman et al., IEEE Trans. Appl. Supercond. **15**, 579-82 (2005).
- [4] F. Marsili et al., Nat. Photonics **7**, 210, (2013).
- [5] G. N. Gol'tsman et al., IEEE Trans. Appl. Supercond. **17**, 246–51 (2007).
- [6] A.D. Semenov, G.N. Gol'tsman and A.A. Korneev, Physica C **351**, 349(2001).
- [7] A. G. Kozorezov, A. F. Volkov, J. K. Wigmore, A. Peacock, A. Poelaert and R. den Hartog, Phys. Rev. B **61**, 11807 (2000).
- [8] A. Engel and A. Schilling, J. of Appl. Phys. **114**, 214501 (2013).
- [9] J. J. Renema, G. Frucci, Z. Zhou, F. Mattioli, A. Gaggero, R. Leoni, M. J. A. de Dood, A. Fiore, and M. P. van Exter Phys. Rev. B **87**, 174526 (2013).
- [10] F. Marsili, M. J. Stevens, A. Kozorezov, V. B. Verma, Colin Lambert, J. A. Stern, R. D. Horansky, S. Dyer, S. Duff, D. P. Pappas, A. E. Lita, M. D. Shaw, R. P. Mirin, and S. W. Nam, Phys. Rev. B **93**, 094518 (2016).
- [11] A. G. Kozorezov, C. Lambert, F. Marsili, M. J. Stevens, V. B. Verma, J. A. Stern, R. Horansky, S. Dyer, S. Duff, D. P. Pappas, A. Lita, M. D. Shaw, R. P. Mirin, and Sae Woo Nam, Phys. Rev. B **92**, 064504 (2015).
- [12] Yu. P. Gousev et al., Appl. Phys. Lett. **75**, 3695 (1994).
- [13] M. Yu. Reizer, Phys. Rev. B **40**, 5411 (1989).
- [14] E.M. Gershenzon et al., JETP Lett. **70**, 505 (1990).
- [15] E. M. Gershenzon et al., JETP Lett. **86**, 758 (1984).
- [16] A. Kardakova, A. Shishkin, A. Semenov, G. N. Goltsman, S. Ryabchun, T. M. Klapwijk, J. Bousquet, D. Eon, B. Sacépé, Th. Klein, and E. Bustarret, Phys. Rev. B **93**, (2016).
- [17] Superconductivity, edited by R. D. Parks Marcel Dekker, New York, Chap. 6 (1969).
- [18] Irwin, K., & Hilton, G., Cryogenic Particle Detection, **63** (2005) .
- [19] S. B. Kaplan et al., Phys. Rev. B **14**, 4854 (1976).
- [20] Philip B. Allen, Phys. Rev. Lett. **59**, 1460(1987).
- [21] Perrin N. Vanneste C. [Journal]. - Paris : Physical Review B (Condensed Matter), Volume 28, Issue 9, 1983.
- [22] S. B. Kaplan, Journal of Low Temperature Physics, V 37, Nos. 3/4, (1979).
- [23] Bergmann G, Wei W, Zou Y and Mueller R M, Phys. Rev. B **41**, 7386 (1990).
- [24] N. G. Ptitsina, Chulkova G. M., Gershenzon E. M., Gershenzon, M. E, JETP Lett. **80**, No. 5, 960 (1995).
- [25] Schmid A “Localization, Interaction, and Transport Phenomena”ed B Kramer, G Bergmann andY Bruynseraede (Berlin: Springer) (1985).
- [26] Reizer M. Yu., A. V. Sergeev, JETP **63**, 616 (1986).
- [27] Lin J Jand J P Bird, J. Phys.: Condens. Matter **14** R501 (2002).
- [28] A. Kardakova al., Appl. Phys. Lett. **103**, 252602 (2013).

Figures captions:

FIG.1. Setup for measuring of τ_{e-ph} (the figure was generated partly using Ref [16, 28]). The sample which is kept at the middle of superconducting transition absorbs radiation at intermediate frequency (IF) from two splitted BWOs mixing on the sample. The inset shows how the change of the electron temperature by absorbed radiation induces the change of sample resistance that consequently generates an output signal which is measured at certain IF by spectrum analyzer. Frequency dependence (solid line - inset of spectrum analyzer) shows the way of choosing value of roll-off frequency at 3 dB level (eq. (1)) which is used to extract τ_R .

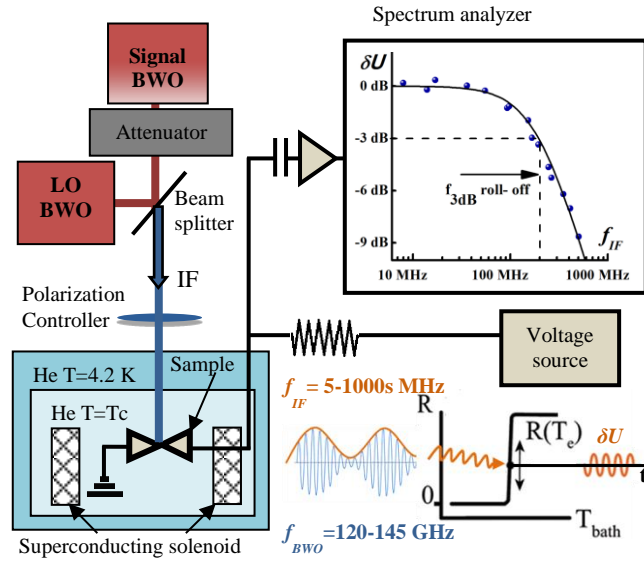


FIG.2 Searching an operation regime with low heating electron subsystem by DC and RF powers. (a) Dependence of measured time, τ_R , on value of DC voltage at low applied RF power (red curve) and on attenuation of incident RF radiation at small value of DC voltage (blue curve). The area where time constant doesn't depend on DC bias voltage and attenuation was found as area with negligible DC and RF heating. The error bars are plotted based on uncertainty of definition the roll-off frequency on spectrum curve. (b) I-V dependence. Dashed and solid curves refer to superconducting transition and superconducting state at $T = 1.8\text{ K}$ correspondingly. The selected area is the operation point.

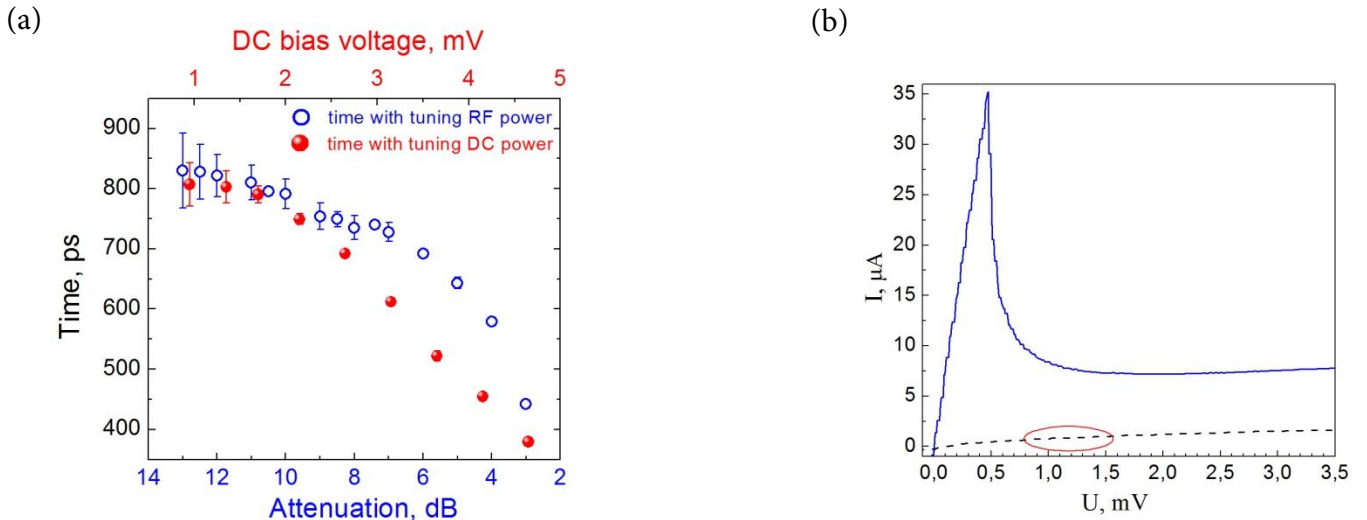


FIG.3 (a) Frequency dependence of the output voltage signal from the WSi microstrip with thickness 3.4 nm for different magnetic fields. The solid curves are the fitting data under the Eq. (1). Introduction of magnetic field shifts spectrum curve to area of low frequencies. (b) Temperature dependence of measured time, τ_R , in double logarithm scale. The solid line is fit according to $\tau_R \sim T^{-n}$ where $n=3$.

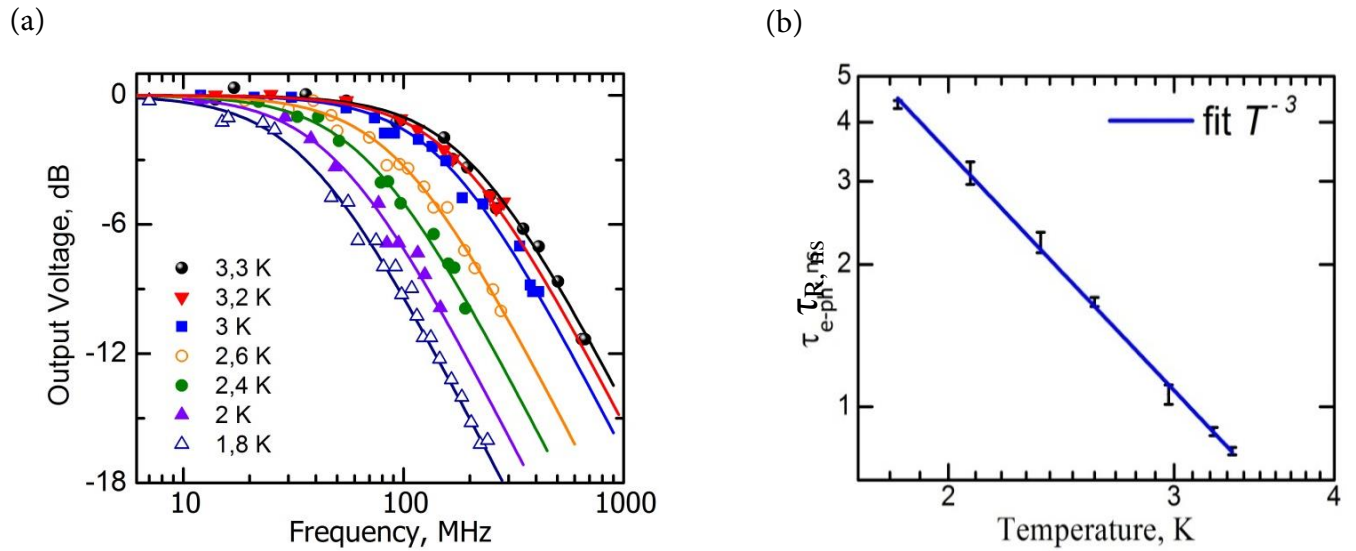


FIG.4 Temperature dependence of the second critical magnetic field used in calculating electron diffusion constant under Eq. (4). The inset shows temperature dependence of sample resistance for different magnetic fields where introduction of magnetic field shifts $R(T)$ curves to low temperatures area.

